BASIC SCIENCE

Nanomedicine: Nanotechnology, Biology, and Medicine
34 (2021) 102373

Original Article

nanomedjournal.com

Blockade of HIF-1α and STAT3 by hyaluronate-conjugated TAT-chitosan-SPION nanoparticles loaded with siRNA molecules prevents tumor growth

Hendrik Setia Budi[a,1], Sepideh Izadi[b,c,1], Anton Timoshin[d], Sima Heydarzadeh Asl[b], Behzad Beyzai[b], Amir Ghaderpour[e], Fatemeh Alian[f], Farzaneh Sadat Eshaghi[g], Seyedeh Mahboubeh Mousavi[b], Behnam Rafiee[h], Afshin Nikkhoo[b], Armin Ahmadi[i], Hadi Hassannia[j], Majid Ahmadi[k], Mozhdeh Sojoodi[l,*], Farhad Jadidi-Niaragh[b,m,**]

[a]*Department of Oral Biology, Faculty of Dental Medicine, Universitas Airlangga, Surabaya, Indonesia*
[b]*Immunology Research Center, Tabriz University of Medical Sciences, Tabriz, Iran*
[c]*Student Research Committee, Tabriz University of Medical Sciences, Tabriz, Iran*
[d]*I.M. Sechenov First Moscow State Medical University (Sechenov University), Department of propaedeutics of dental diseases, Moscow, Russia*
[e]*Medical Biology Research Center, Kermanshah University of Medical Sciences, Kermanshah, Iran*
[f]*Institute of Biochemistry and Biophysics, University of Tehran, Tehran, Iran*
[g]*Department of Genetics, Faculty of Medicine, Shahid Sadoughi University of Medical Sciences, Yazd, Iran*
[h]*Department of Pathobiology, Faculty of Veterinary Medicine, Shahrekord University, Shahrekord, Iran*
[i]*iepartment of Chemical and Materials Engineering, The University of Alabama in Huntsville, AL, USA*
[j]*Immunogenetic Research Center, Faculty of Medicine, Mazandaran University of Medical Sciences, Sari, Iran*
[k]*Stem Cell Research Center, Tabriz University of Medical Sciences, Tabriz, Iran*
[l]*Division of Surgical Oncology, Massachusetts General Hospital Cancer Center and Harvard Medical School, Boston, USA*
[m]*Department of Immunology, School of Medicine, Tabriz University of Medical Sciences, Tabriz, Iran*

Revised 15 December 2020

Abstract

HIF-1α and STAT3 are two of the critical factors in the growth, proliferation, and metastasis of cancer cells and play a crucial role in inhibiting anti-cancer immune responses. Therefore, we used superparamagnetic iron oxide (SPION) nanoparticles (NPs) coated with thiolated chitosan (ChT) and trimethyl chitosan (TMC) and functionalized with hyaluronate (H) and TAT peptide for delivery of siRNA molecules against STAT3 and HIF-1α to cancer cells *both in vivo* and *in vitro*. The results indicated that tumor cell transfection with siRNA-encapsulated NPs robustly inhibited proliferation and migration and induced apoptosis in tumor cells. Furthermore, simultaneous silencing of HIF-1α and STAT3 significantly repressed cancer development in two different tumor types (4T1 breast cancer and CT26 colon cancer) which were associated with upregulation of cytotoxic T lymphocytes and IFN-γ secretion. The findings suggest inhibiting the HIF-1α/STAT3 axis by SPION-TMC-ChT-TAT-H NPs as an effective way to treat cancer.

Key words: Hypoxia inducible factor; STAT3; SPION; Chitosan; Nanoparticle; Hyaluronate

Support: This study was supported by the National Institute for Medical Research Development (NIMAD; grant number: 989658) and Tabriz University of Medical Sciences (grant numbers: 62447 and 62482).
Conflict of Interest: There is no conflict of interest.
* Correspondence to: M. Sojoodi, Division of Surgical Oncology, Massachusetts General Hospital Cancer Center and Harvard Medical School, Boston, USA.
** Correspondence to: F. Jadidi-Niaragh, Immunology research center, Tabriz University of Medical Sciences, Tabriz, Iran.
E-mail address: jadidif@tbzmed.ac.ir. (F. Jadidi-Niaragh).
[1] These authors equally contributed in this study.

https://doi.org/10.1016/j.nano.2021.102373
1549-9634/

Please cite this article as: Budi HS, et al, Blockade of HIF-1α and STAT3 by hyaluronate-conjugated TAT-chitosan-SPION nanoparticles loaded with siRNA molecules prevents tumor growth. *Nanomedicine: NBM* 2021;34:102373, https://doi.org/10.1016/j.nano.2021.102373

The interactions of tumor cells with their microenvironmental ingredients, including stromal cells, extracellular matrix elements, immunosuppressive cells, and soluble factors lead to the clonal development, metastasis, and progression of neoplastic cells.[1] Therefore, the management of the tumor microenvironment can inhibit cancer progression by stimulating the anti-tumor immune responses and preventing the growth of neoplastic cells.[2,3] Accordingly, our recent experience has shown that targeted changes in tumor microenvironment can be an intelligent strategy to inhibit tumor growth and spread by reducing mechanisms that suppress anti-tumor immune responses.[4–8] The main characteristics of the tumor's metabolic microenvironment include extracellular acidosis, increased adenosine and lactate concentrations, and most importantly decreased oxygen levels (anoxia, hypoxia). Hypoxia-inducible factor (HIF)-1α, which is normally degenerated under normoxic circumstances, is stabilized in the hypoxic microenvironment.[9] The stabilized HIF1α protein is transported to the nucleus and dimerized with ARNT to form the HIF1 complex (HIF1α/ARNT).[10,11] HIF1 activates genes participated in glycolysis, cellular proliferation, metastasis, and neovascularization through connecting to HIF-binding sites.[12] Besides, the increased activity of signal transducers and transcription activator-3 (STAT3) has been shown in several solid tumors such as lung, kidney, breast, head/neck, and prostate tumors. STAT3 activity in normal cells is completely controlled by the accessibility of growth factors (PDGF, EGF, *etc.*) and cytokines (IL-10, IL-6, *etc.*), whereas in tumor cells, the expression of STAT3 activators such as IL-10 and IL-6 is increased by stromal and cancer cells in the tumor microenvironment.[13] STAT3 enhances tumor growth by binding to promoters of genes involved in proliferation (Cyclin D1), apoptosis (Mcl1, BCL-2, Survivin, and Bcl-xL), and angiogenesis (VEGF).[14,15] Recent studies have shown that hypoxic conditions lead to STAT3 activation in a number of tumor cells and animal models.[16,17] On the other hand, activated STAT3 up-regulates the expression of HIF-1α by enhancing the transcriptional activity and stability in the hypoxic tumor milieu.[18] Given the coexistence of hypoxic and inflammatory microenvironments in solid tumors and activation of STAT3 under hypoxic milieu, it is assumed that STAT3 is one of the main factors induced by hypoxic tumor microenvironment. Accordingly, knockdown of HIF-1α and STAT3 could be an efficient anti-cancer curative strategy.[19] In the current study, we applied siRNA technology to inhibit STAT3 and HIF1α molecules and a nano-based delivery system to transfer these siRNAs to tumor cells. Superparamagnetic iron oxide nanoparticles (SPIONs) are of the highly efficient nano-based carriers for delivery of anti-cancer therapeutics, which exhibit excellent features for cancer therapy such as low immunogenicity, biodegradability, low toxicity, biocompatibility, high refractive index, high surface to volume proportion, and ease of separation.[20,21] In addition to the listed benefits, features such as non-specific binding to serum proteins and rapid clearance from the bloodstream are limitations of SPIONs. Although we did not use the magnetic properties of generated NPs in this study, it is possible that this property of nanocarriers could also be used in combination therapies. To increase the stability of SPIONs and also to improve their performance and efficiency, SPIONs can be encapsulated with various types of synthetic and natural polymers such as chitosan, dextran, polyethylene glycol, and alginate.[22] In this study, we used trimethyl chitosan (TMC), thiolated chitosan (ChT), and hyaluronate (H) to coat SPIONs. Coating of SPIONs with chitosan derivatives (ChT and TMC) increases siRNA loading potential because of the high positive charges (27, 28). On the other hand, the use of H polymer in the NP structure increases the cellular uptake of NPs through interacting with the CD44 molecule expressed in many cancer cells.[23] Also, conjugation of NPs with TAT peptides as the cell-penetrating peptides (CPPs) is done to better transport therapeutic molecules (siRNA and drug) through the lipophilic barrier of cell membranes and transfer them to cancer cells while maintaining biological activity.[24] In the present study, we suggested a novel anti-cancer therapeutic strategy based on the simultaneous suppression of HIF-1α and STAT3 using SPION-TMC-ChT-TAT-H NPs in breast and colorectal tumor cell lines for the first time.

Methods

Reagents

Chitosan (MW: 120 kDa, DD: 95%) and hyaluronan were bought from Sigma (St. Louis, USA). Sodium azide (NaN3), sodium iodide (NaI), and EDC [1-ethyl-3-(3-dimethyl aminopropyl) carbodiimide] were purchased from Merck (Darmstadt, Germany). The synthetic TAT peptide (C (Npys) GRKKRRQRRR, purity: 93%) was taken from TAG Copenhagen (Copenhagen, Denmark). The MTT assay kit was bought from Sigma-Aldrich (Mannheim, Germany). HIF-1α and STAT3 specific siRNAs, and control siRNA were bought from Santa Cruz (Santa Cruz, CA, USA).

Mice & cell lines

The murine colorectal cancer cell line (CT26) and mouse breast cancer cells (4T1) were purchased from the Pasteur Institute (Tehran, Iran). The cells were cultured in culture media (Gibco, Paisley, UK) enriched with FBS (10%) and antibiotics (streptomycin/penicillin) and were kept in the incubator (5% CO2, 37 °C). BALB/c mice (8 weeks, female) were bought from Pasteur Institute (Tehran, Iran) and kept in the standard conditions. Animal tests were carried out based on the Ethics Committee's Guide of Tabriz University of Medical Sciences. After injecting tumor cells (6.5×10^5) subcutaneously into the right flanks, the tumors were formed and two days later the tumor size was examined, as described previously.[25,26]

Generation of iron oxide (Fe3O4) nanoparticles

As previously described, the synthesis of SPION was performed using the coprecipitation method.[27] Summarily, 0.4 g FeCl3·6H2O and of 0.15 g FeCl2·4H2O were mixed in a beaker containing100 ml of deionized water under nitrogen atmosphere at 70 °C. In the next step, ammonium hydroxide 25% was added drop by drop to this solution to increase the pH to 11 and the mixture was stirred at this temperature for 1 h. Then, the resulting precipitate was separated from the reaction medium by a magnetic field and washed four times with

deionized water until the pH of the solution reaches 7. Ultimately, the obtained Fe3O4 NPs dried in a vacuum oven at 40 °C.

Generation of TMC

Trimethyl chitosan was constructed based on our previously described protocols.[28] Briefly, chitosan (0.7 g) and NaI (1.5 g) were dissolved in 25 ml of N-methyl-2-pirrolidone (NMP) solvent at 60 °C. Afterward, NaOH (2.7 ml) and CH3I (3 ml) were added and the solution was stirred for 5 h at 60 °C. Then the TMC iodide precipitate formed by adding acetone was separated by centrifugation (18,000 rpm, 5 min). To substitute chloride ions with iodide ions, the resulting precipitate was dissolved in NaCl solution. Ultimately, the obtained mixture was first dialyzed and then lyophilized.

Thiolation of chitosan

Synthesis of thiolated chitosan was performed according to our previous report.[29] Briefly, chitosan (500 mg) was solved in the hydrochloric acid and deionized water under stirring. In the next step, first thioglycolic acid (TGA) and then EDC were added and the resulting solution was incubated for 4 h in a dark environment. The mixture (pH 5) was then dialyzed using HCl 1 M containing NaCl and DI water to remove free elements. Eventually, the thiolated chitosan solution was lyophilized.

Preparation of SPION-TMC-ChT-TAT-H NPs loaded with siRNA

In the first step, TMC solution (200 μl, 0.5 mg/ml) and ChT solution (100 μl, 1 mg/ml) were added to the aqueous solution of iron oxide NPs (solved in distilled water) and stirred in a lightless environment for 24 h. The coating of SPION with TMC and ChT occurred through electrostatic reactions. Afterward, the solution of TAT peptide was added to the previous mixture and stirred at 250 g for 24 h. The last step of the synthesis and design of NPs was performed by adding hyaluronate solution (100 μl, 1 mg/ml) to SPION-TMC-ChT-TAT NPs solution. SiRNA loading in NPs was performed based on the ionic gelation protocol. Therefore, 2.5, 5, 10, 15, and 20 μg of siRNA were mixed with SPION-TMC-ChT-TAT-H NPs solution, vortexed (20 s), and then incubated in at 25 °C for 2 h. The formation of siRNA-NPs complex was investigated using electrophoresis on 2% agarose gel.

Particle size & zeta potential measurements

The zeta potential (ξ), average particle size, and polydispersity index (PDI) of NPs were specified using a Dynamic Light Scattering (DLS, Zs90, Malvern, United Kingdom). The experiment was accomplished at a wavelength of 633 nm and a 90° detection angle at 25 °C.[30]

FTIR spectroscopy

The FT-IR Spectrometer (Magna IR 550; Madison, WI) was used to determine the chemical structure of generated NPs. Briefly, NPs were freeze-dried and embedded in potassium bromide (KBr) pellets and the transmission spectra were seized with a 4 cm^{-1} resolution at 4000-425 cm^{-1}.[31]

Transmission electron microscopy (TEM)

In order to confirm the shell core presence and the shell thickness, TEM images of the samples were obtained using JEOL 2010 FX at an accelerating voltage of 150 kV. The images were taken after spreading the dried powder of the samples on the lacey carbon grids.

X-ray diffraction (XRD) analysis

To ascertain the crystal structure of the SPIONs by XRD, Bruker D8 Advance diffractometer with Copper K-α radiation (wavelength of 1.5406 Å) operating at 40 kV and 30 mA was used.

Thermogravimetric analysis (TGA)

TGA measurements were performed using the Q500 TA instrument with a heating rate of 20 °C min^{-1} under constant flow of nitrogen. Prior to TGA experiments, all samples were freeze and dried. After that, at 120 °C, the samples were heated evenly for 10 min to entirely evaporate the water molecules and other volatiles remaining in the sample. TGA diagrams of polymers were obtained to measure weight changes as a function of temperature.

Cellular uptake study

Briefly, CT26 and 4T1 cells (1×10^5cells per well) were plated in the 6-well plate. After 24 h, cell treatment was accomplished with FITC-siRNA loaded SPION-TMC-ChT-TAT-H NPs, FITC-siRNA loaded SPION-TMC-ChT-TAT, and FITC-siRNA-loaded SPION-TMC-ChT NPs and incubated for 24 h. In the next step, the cells were fixed using the formaldehyde solution for 30 min. Subsequently, the cells were observed using confocal microscopy (Nikon ECLIPSE Ti, Tokyo, Japan). Furthermore, the efficacy of transfection was also examined using flow cytometry. At first, cells were plated in the 6-well plate, incubated until 60% confluence, and transfected with FITC-labeled-TAT-H-NPs, FITC-loaded-TAT-NPs, and TAT/H free NPs. After trypsinization and washing of cells with PBS, the transfection efficacy was evaluated by using the flow cytometry (Becton-Dickenson, Mountain View, CA, USA).[32]

Calculation of siRNA loading efficiency

In order to evaluate the loading capacity of siRNA in SPION-TMC-ChT-TAT-H NPs, the concentration of siRNA in the collected supernatant after centrifugation (15,000 rpm, 15 min) was measured. The amount of free siRNA in the supernatant was assessed according to the absorbance obtained at 270 nm. The SiRNA loading efficiency was calculated using the following formula[33]:

$$\text{Loading efficiency (\%)} : [1-(\text{OD siRNA in the supernatant}/\text{OD initial amount of siRNA})] \times 100$$

Stability assay

The gel electrophoresis technique was applied to examine the stability of SPION-TMC-ChT-TAT-H NPs in serum. At first,

siRNA loaded SPION-TMC-ChT-TAT-H NPs were mixed with FBS under mild shaking at 37 °C. Afterward, a little amount of each sample was gathered at specific times (2, 4, 6, 12, 18, 24, and 32 h) and stored at −20 °C until the moment of electrophoresis implementation.

SiRNA release profile

The analysis of the siRNA release from nanocarriers *in vitro* was performed according to previous studies. Briefly, nanocarrier-siRNA was dissolved in PBS and transferred to a dialysis bag (cut-off: 15 K). After that, the dialysis bag was immersed in a beaker filled with PBS as a release medium with PH of 6 and 7.4. The dialysis was carried out under shaking (90 rpm) at 37 °C. Finally, at certain times (2, 4, 8, 12, 18, 24, 36, and 48 h), some of the released PBS was gathered and the absorbance of siRNA was measured using the UV–vis spectrometry.[9]

Cytotoxicity assay

The viability of CT26 and 4T1 cell lines after exposure to different therapeutic formulations was assessed using the MTT assay.[34] Both 4T1 and CT26 cells (10^4 cells per well) were cultured in the 96-well plate. After 24 h, the cultured cells were treated with NPs, siRNA HIF-1α- loaded NPs, siRNA STAT3-loaded NPs, and siRNA HIF-1α/siRNA STAT3 loaded NPs for 24 or 48 h. Afterward, the elementary medium replaced with fresh RPMI and MTT solution (10 μl/well, 5 mg/ml) was added and incubated for 3 h. After adding DMSO (150 μl), the ELISA Plate Reader (Organon Teknika, Turnhout, Belgium) was used to examine the viability of tumor cells at 570-630 nm.

Wound healing assay

The scratching method based on our previous reports was used to study cell migration.[35] In general, the cells were seeded in 6-well plates and then incubated until 75% confluence. After that, cells were scratched using pipette tips and then treated with siRNA-loaded NPs. Finally, at the appointed times, the images of scratched areas was obtained using an inverted microscope and examined with Image J software.

CDNA synthesis and qPCR

Firstly, total RNA was extracted from 4T1 and CT26 cancer cells transfected with siRNA-loaded NPs, according to the PrimeScript® RT reagent Kit instructions (Takara Bio Inc., Shiga, Japan). Synthesis of cDNA from 500 ng of the whole isolated RNA was conducted using QuantiTect Reverse Transcription kit. The qPCR was carried out by PCR Master Mix (SYBR Green, Thermo Scientific). Amplification reactions were done in a total volume of 20 μl by using the StepOne Real-Time PCR System (Applied Biosystems Inc., Carlsbad, CA, USA). The formula $2^{-\Delta\Delta CT}$ was used to calculate the expression of target genes and the beta-actin was used as a control.[36] Specific primers used for qPCR are demonstrated in Table 1.

Western blotting

Briefly, cells treated with different treatment groups including siRNA HIF-1α loaded NPs, siRNA STAT3 loaded NPs, and siRNA HIF-1α/STAT3 loaded NPs. After cell treatment, Western blot analysis was carried out similar to our previous reports.[37] 24 h after incubation with primary antibodies such as anti-HIF-1α, anti-STAT3, anti-Bcl2, anti-Ki-67, anti-MMP2, anti-MMP9, and anti-β-actin, the membrane was reincubated with secondary antibodies for 1 h. At the end, ECL kit (Pierce Biotechnology) was used to visualize the bands.

Bürker chamber assay

To count 4T1 and CT26 cancer cells transfected with siRNA-loaded NPs, cell suspension (20 μl equal 200 cells/square) was added between the hemocytometer (Neubauer chamber) and cover glass using Gilson Pipetman P20 Single Channel Pipette. Finally, the number of cells in each of the four outer squares was counted and their concentration was calculated using the following formula[38]:

$$\left[{}^{\text{Cell/ml}}\right] = \frac{\text{Cell counted (4 large squares)}}{4} \times (\text{dilution factor}) \times 1 \times 10^4$$

BrdU assay

The BrdU Cell Proliferation ELISA kit (Thermo Fisher Scientific, MA, USA) was utilized to study the inhibitory impact of siRNA-loaded NPs on cancer cell proliferation. Briefly, CT26 and 4T1 cells (5×10^3cells per well) were cultured in 96-well plates and incubated overnight. Afterward, Brdu solution (10 μl per well) was added and incubated for 4 h. The cells were then transfected with mouse anti-BrdU Ab conjugated to HRP (100 μl/well) for 90 min. In order to remove free mAbs, washing was performed, and then tetramethylbenzidine was added (100 μl per well). After 30 min, H2SO4 solution was used to stop the reaction, and then the adsorption at 600 nm was measured using ELISA Plate Reader.

Cytokine quantification by ELISA

To measure the cytokine secreted by T cells extracted from tumor of 4T1 and CT26 tumor-bearing mice, 10^6 T cells were incubated with 80 μg/ml of tumor cell lysate (TCL) and then complete culture medium (1 ml/well) at 37 °C and 5% CO2. After 72 h, the supernatants were collected and secretion of IFN-γ was examined based on the manufacturer's instructions of ELISA kit (Invitrogen, Carlsbad, CA, USA).

Flow cytometry

As previously described, the frequency of $CD8^+$ T cells and $CD8^+$ $CD44^+$ T cells was ascertained by flow cytometry using CD8-FITC, CD44-PE and isotype control mAbs (Biolegend, CA, USA).[39] Summarily, 10^6 cells were suspended in staining buffer (50 μl) and transfected with fluorochrome-labeled mAbs (30 min, 4 °C). The stained cells were washed and investigated using BD FACS Calibur flow cytometer (Becton-Dickenson) and FLOWJO software.

Table 1
Sequences of primer.

Gene name	Forward	Reverse
Bcl-2	5′-GGCTGGGGATGACTTCTCTC-3′	5′-ACAATCCTCCCCCAGTTCAC-3′
β-actin	5′-GGTCATCACTATTGGCAACG-3′	5′-ACGGATGTCAACGTCACACT-3′
Ki-67	5′-AGAGCCTTAGCAATAGCAACG-3′	5′-GTCTCCCGCGATTCCTCTG-3′
HIF-1α	5′-AGCAGGAATTGGAACATTATTGCAG-3′	5′-TGTGGTAATCCACTCTCATCCATTG-3′
STAT3	5′-CACGAAAGTCAGGTTGCTGGT-3′	5′-ACTTTTGTGTTCGTGCCCAGA-3′
MMP2	5′-TGTGTCTTCCCCTTCACTTT-3′	5′-GATCTGAGCGATGCCATCAA-3′
MMP9	5′-ACACGACATCTTCCAGTACC-3′	5′-CAGGAGGTCGTAGGTCACGTAGC-3′

In vivo anti-tumor efficacy

To investigate the antitumor effect of siRNA-loaded nanocarriers, inhibition of tumor growth was performed *in vivo*. As mentioned before to form a tumor model, 6.5×10^5 cells from each cell line (4T1 and CT26) were injected subcutaneously into the right flank of BALB/c mice. Subsequently, tumor-inoculated mice have randomly received treatment groups including 1) NP-siRNA HIF-1α, 2) NP- siRNA STAT3, 3) NP-siRNA HIF-1α + STAT3, and 4) saline (control). Treatments were administrated intravenously in a total volume of 100 μl for NPs and 10 μg for siRNA. Besides, mice were followed to determine changes in tumor volume for 60 days and to determine survival rates for 90 days. Biodistribution of CY-5 labeled siRNA-loaded NPs in both tumor models was also evaluated by using *in vivo* imaging technique, as described previously.[4,7]

Statistical analysis

The experimental result analysis was conducted using GraphPad Prism software. Significance level prediction was carried out by one-way ANOVA. P value < 0.05 was considered significant. All experiments were repeated at least twice. Bar charts in the results indicate mean values of data ± standard error of means (SEM). Moreover, * demonstrates $P < 0.05$, ** indicates $P < 0.01$, and *** represents $P < 0.001$.

Results

Characterization of NPs

The DLS results showed that produced NPs were about 118 nm in size, with PDI <0.25 and surface charge (ζ) of 20 mV (Figure 1, *A* and *B*). Furthermore, size and zeta potential data of all nanostructures including SPIONs, SPIONs-TMC, SPIONs-TMC-ChT, SPIONs-TMC-ChT-TAT, SPIONs-TMC-ChT-TAT-HA were provided in Table 2. Proper size and positive charge of particles cause the optimal transfer of siRNA to tumor cells. Also, the amount of zeta potential less than +30 mV provides sufficient repulsive force to achieve better colloidal stability of the NPs. The zeta potential is an indication of the surface potential, and so determines the magnitude of the electrical double layer repulsion. The total interaction between particles is the sum of the electrical double layer and the van der Waals interaction which is determined by the magnitude of the Hamaker constant of the material and the difference in the refractive index between the particle and solvent. A zeta potential of less than 30 mV is usually (not always) adequate to prevent the capsule accumulation.

The successful binding of thiol (-SH) groups to the chitosan molecules was confirmed by the FTIR spectroscopy of chitosan and the synthesized NPs (Figure 1, *C*). Contrary to the chitosan spectrum diagram, a different band at 1750 cm^{-1} appeared in the spectrum of ChT which was assigned to –SH groups. Moreover, the presence of a peak at 1650 cm^{-1}, relevant to the –OH (hydroxyl) groups, confirmed the correct binding of hyaluronate to chitosan and formation of ChT-H NPs.

The capacity of SPION-TMC-ChT-TAT-H nanocarriers for siRNA loading was studied by gel electrophoresis. In brief, 2.5, 5, 10, 15, and 20 μg of siRNA was used for loading by synthesized nanocarriers. As shown in Figure 1, *D*, the nanocarriers were able to encapsulate up to 15 μg of siRNA.

In vitro stability of siRNA-loaded SPION-TMC-ChT-TAT-H NPs was examined using the gel electrophoresis after dissolving the NPs in FBS at certain times (2, 4, 8, 12, 18, 24, 36, and 48 h). The results demonstrated that the release of siRNA started after 18 h and lasted for 48 h (Figure 1, *E*).

The siRNA release pattern was used to investigate the release rate of siRNA in PBS with pH 6 and 7.4. The results illustrated that the siRNA release happened gently during the 36 h and attained the steady-state after 48 h (Figure 1, *F*).

HIF-1α & STAT3 expression was repressed by siRNA-encapsulated NPs

Cellular uptake of nanocarriers was conducted by transfecting carcinoma cells with FITC-labeled siRNA-loaded SPION-TMC-ChT-TAT-H. As exhibited in Figure 2, *A*, cells transfected with FITC-labeled siRNA loaded NP-TAT-H and NP-TAT generated more powerful green fluorescent signals than cells exposed to unmodified NPs, indicating the great potential of TAT and HA conjugated NPs to penetrate malignant cells. Flow cytometry evaluation demonstrated that 83% of the cells were transfected with NP-TAT-HA, 68% with NP-TAT, while 15% of the cells were transfected with unmodified NPs. Therefore, our results confirmed that the cell adsorption of NPs coated with TAT and H is much higher than that of uncoated NPs (Figure 2, *B*).

Thereafter, the potency of siRNA-loaded NPs in the suppression of HIF-1α and STAT3 mRNA expression levels in both cell lines was evaluated by the qPCR method. The results indicated that HIF-1α-specific siRNA-loaded SPION-TMC-ChT-TAT-H NPs greatly reduced the HIF-1α expression in

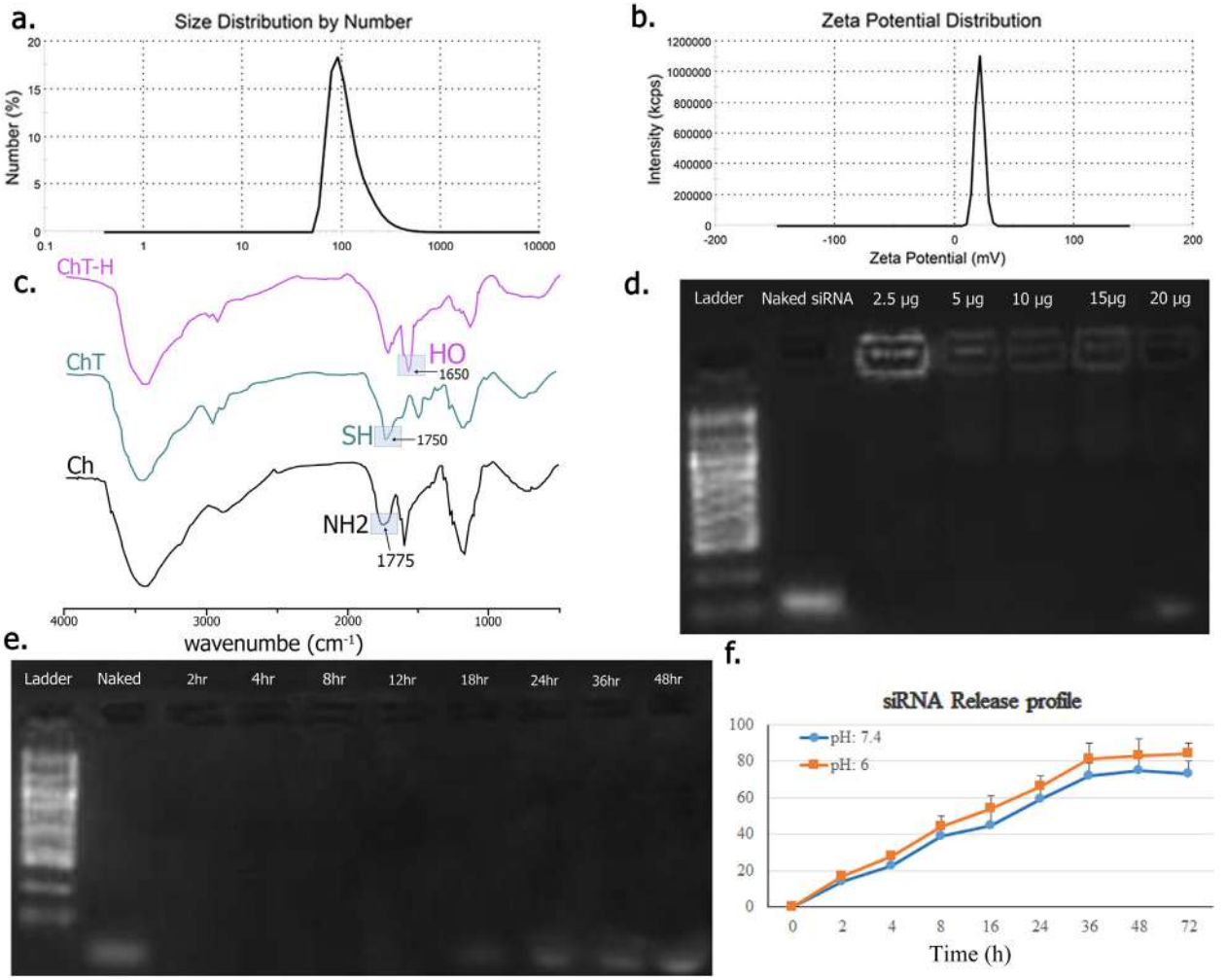

Figure 1. Physicochemical properties of SPION-TMC-ChT-TAT-H NPs. Produced NPs showed a size of 118 nm and ζ potential value of 20 mV **(A, B)**, and PDI < 0.25. The IR spectra proved the correct formation of the NPs **(C)**. The capacity of NPs for siRNA encapsulation evaluated; Lane 1: naked siRNA, Lane 2: 2.5 µg, Lane3: 5 µg, Lane 4: 10 µg, Lane5: 15 µg, and Lane 6: 20 µg **(D)**. The stability of siRNA-loaded NPs by using the gel electrophoresis is depicted **(E)**. The siRNA release pattern of NPs was shown in both neutral and acidic conditions **(F)**.

Table 2
The size, PDI, and zeta potential of generated NPs.

Compound	Size (nm)	PDI	Zeta potential (mV)
SPION	49 ± 1	0.165 ± 0.02	−1.98 ± 0.32
SPION-TMC	63 ± 2	0.27 ± 0.03	23.7 ± 1
SPION-TMC-ChT	100 ± 3	0.3 ± 0.05	25 ± 2
SPION-TMC-ChT-TAT	103 ± 4	0.3 ± 0.07	28 ± 3
SPION-TMC-ChT-TAT-H	118 ± 4	0.25 ± 0.06	20 ± 1

4T1 and CT26 cell lines. Besides, the same results were taken from the treatment of 4T1/CT26 cells with STAT3-siRNA encapsulated NPs. In general, siRNA-encapsulated NPs reduced HIF-1α and STAT3 expression (Figure 2, *C*), while other formulations such as blank NPs, naked siRNA, and control siRNA-loaded NPs had no considerable influence on the expression of STAT3 and HIF-1α.

The protein expression of target molecules was also studied using the western blot analysis. Thus, the protein expression of HIF-1α /STAT3 in treated cell lines was meaningfully lower than in untreated cells. Consequently, the highest inhibitory effect was seen in cell lines treated with siHIF-1α + siSTAT3- loaded SPION-TMC-ChT-TAT-H nanocarriers (Figure 2, *D* and *E*)

Co-silencing of HIF-1α/STAT3 reduced the cancer cell viability and invasion

The cellular toxicity of the studied nanocarriers was investigated by the MTT technique. As presented in Figure 3, *A*, the blank SPION-TMC-ChT-TAT-H NPs had no meaningful toxicity effect on tumor cells after 24 h and even 48 h. Though, the combination therapy group, si HIF-1α + si STAT3-loaded NPs, greatly reduced the survival of cells after 24 and especially 48 h, which was due to the simultaneous inhibition of HIF-1α and STAT3 genes.

To investigate the inhibitory impact of SPION-TMC-ChT-TAT-H NPs on the proliferation of cultured cells, *in vitro* BrdU cell proliferation assessment was conducted. The outcomes of

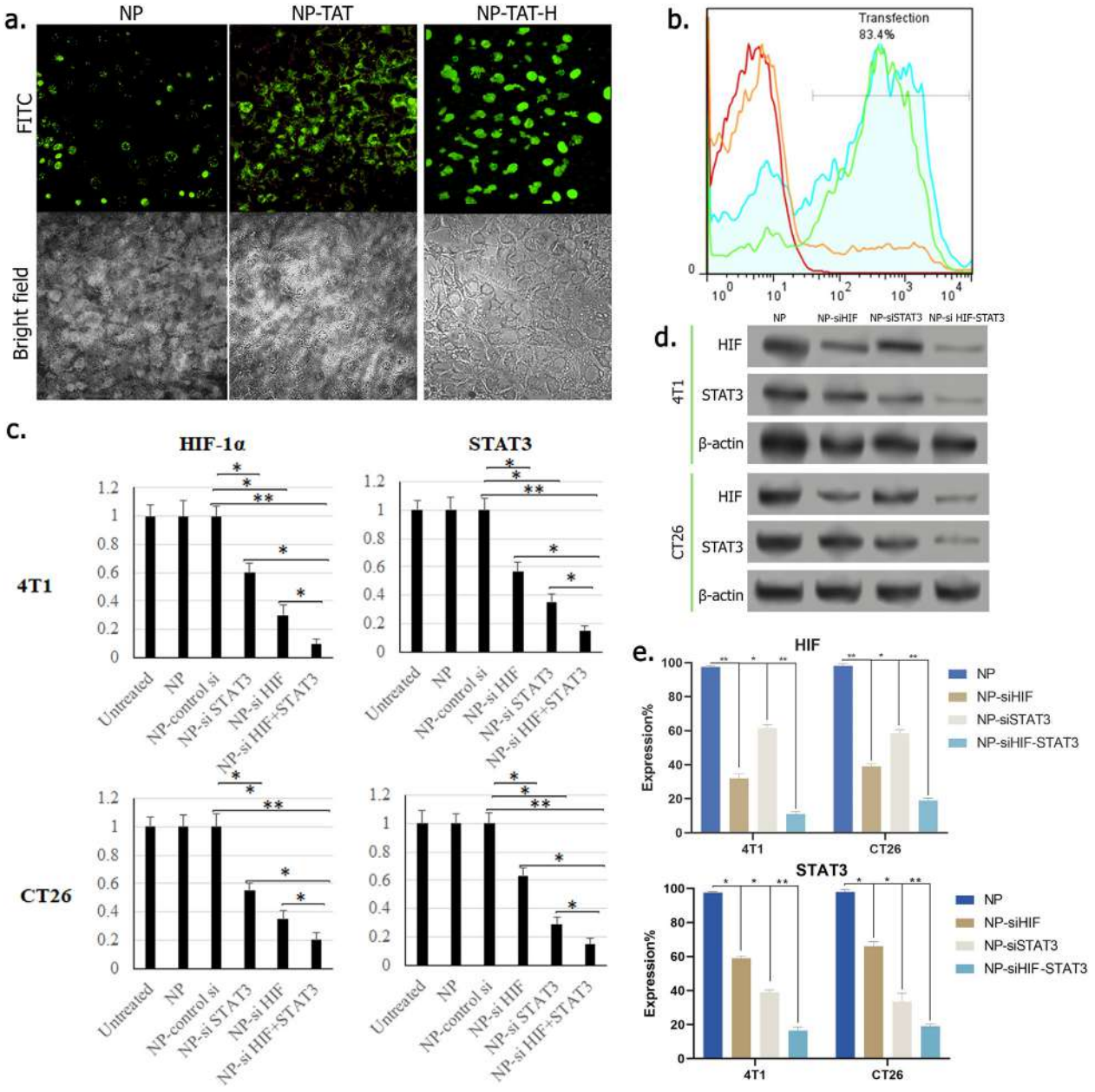

Figure 2. SPION-TMC-ChT-TAT-H NPs efficiently internalized by neoplastic cells and inhibited the expression of target genes. As shown by confocal microscopy **(A)** and flow cytometry **(B)**, the NP uptake by tumor cells markedly increased after conjugation with TAT peptide and H. Neoplastic cells were transfected with FITC-loaded NPs. The levels of mRNA and protein related to HIF-1α and STAT3 were investigated by qPCR assay **(C)** and Western blot analysis **(D** and **E)**, respectively.

this experiment determined that Inhibition of either HIF-1a or STAT3 molecules was able to significantly inhibit cancer cell proliferation; however, the highest anti-proliferative effect was observed after combination therapy in both cell lines (Figure 3, *B*).

In the following step, the *in vitro* Bürker chamber assay was used to examine the monitoring of cell proliferation rate. The results of counting invasive cells under the influence of treatment groups indicated that the simultaneous suppression of HIF-1α and STAT3 molecules using siRNA-loaded SPION-TMC-ChT-TAT-H NPs had the greatest effect in inhibiting the number of invasive cells (Figure 3, *C*).

To investigate the mechanism by which siRNA-loaded NPs exert their pro-apoptotic and anti-proliferative effects, we evaluated the expression of molecules involved in the survival (Bcl-2) and proliferation (Ki-67) in cancer cells. Therefore, to evaluate the therapeutic consequences of NP-siRNA on the action of anti-apoptotic molecules, mRNA and protein levels of Bcl2 molecule were examined. The results proved that concomitant inhibition of HIF-1α and STAT3 by decreasing the Bcl-2 mRNA (Figure 3, *D*) and protein (Figure 3, *F*) expression diminished the resistance of cancer cells to apoptosis. The influence of siRNA loaded nanocomplex on proliferation

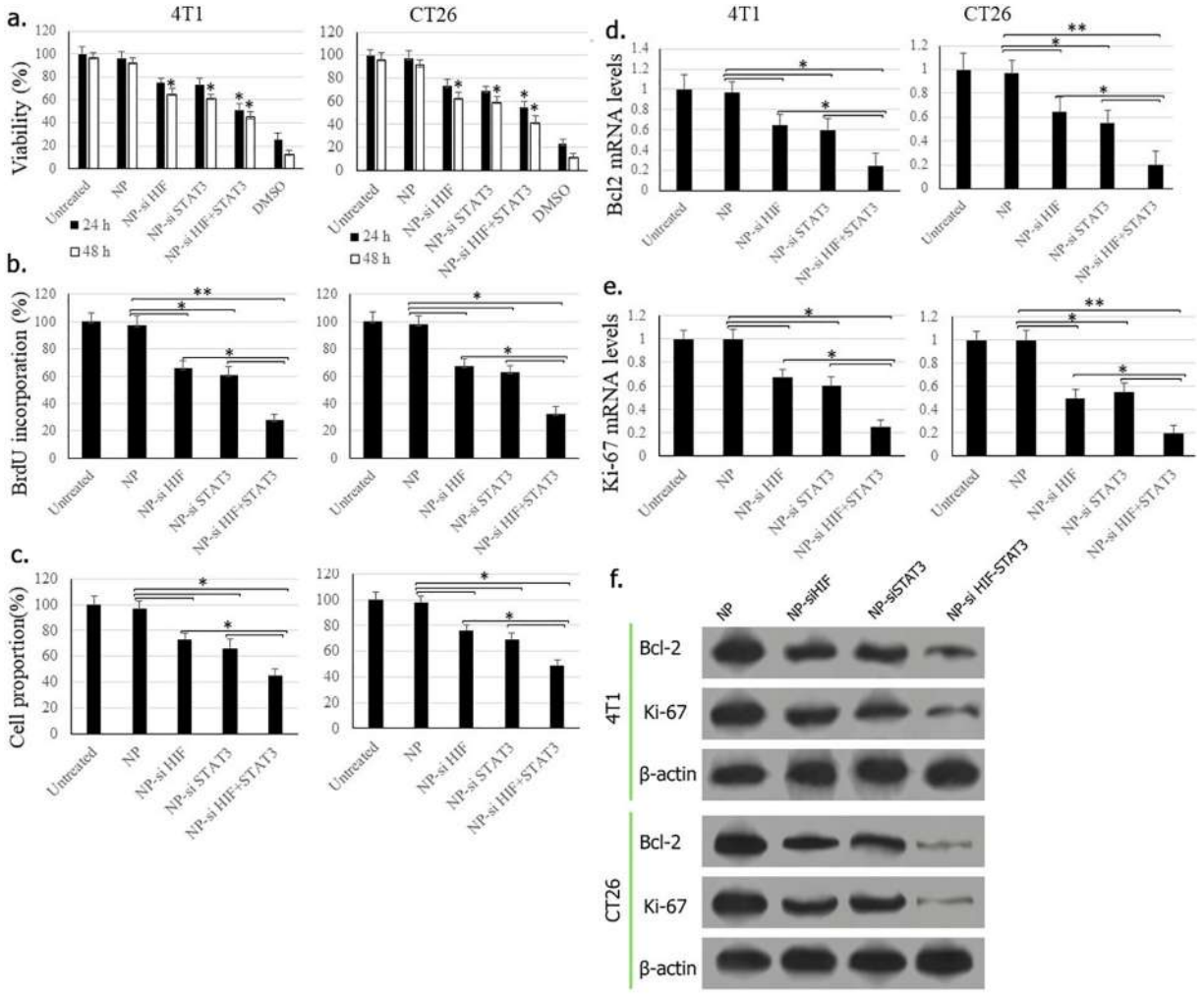

Figure 3. NPs loaded with HIF-1α and STAT3 siRNAs reduced the viability and proliferation of cancer cells. Bar charts demonstrated the mean viability levels of cancer cells after treatment with NP-siRNAs **(A)**. The proliferation of treated 4T1/CT26 cells with different therapeutic groups was examined using the BrdU incorporation assay **(B)**. The enumeration and the proportion of cancer cells were also investigated by the Bürker chamber assay **(C)**. The mRNA and protein levels of anti-apoptotic factor Bcl2 and proliferative factor Ki-67 were examined in both treated cells **(D-F)**.

rate was investigated by measuring the mRNA/protein expression of nuclear proliferative marker, Ki67 antigen. As shown in Figure 3, *E* and *F*, targeting HIF-1α and STAT3 through reducing Ki-67 expression suppresses the potential of tumor cells to proliferate.

Downregulation of HIF-1α and STAT3 reduced the tumor cell migration

The potential migration ability of the malignant cells is a key feature in the induction of metastasis, which was evaluated using scratch assay in both 4T1 and CT26 cell lines. The findings of this experiment demonstrated that repression of HIF-1α and STAT3 alone could decrease cell migration, but minimal cell migration was observed in the concomitant inhibition of STAT3 and HIF-1α in tumor cells. Also, the greatest inhibitory effect was found out in 4T1 breast cancer cell migration (Figure 4, *A* and *B*).

To further investigate cell migration in malignant cells, the expression of MMP2/9 was evaluated as precursors of metastasis. The mRNA levels of MMP2 and MMP9 were diminished considerably in siRNA HIF-1α + siRNA STAT3-SPION-TMC-ChT-TAT-H NPs treated groups, which were consistent with the results of the scratch assessment (Figure 4, *C*). The similar results were observed when the impact of siRNA-loaded NPs was evaluated in the protein expression levels of MMP2/9 (Figure 4, *D* and *E*).

HIF-1α/STAT3 blockage increased CTL activation and survival rate in tumor bearing mice

To investigate the *in vivo* biodistribution of NPs, CY-5-labeled siRNA-loaded NPs were injected intravenously into tumor-bearing mice and biodistribution of NPs was evaluated over time. The results showed that NPs were preferentially accumulated in the tumor site during 48 h (Figure 5, *A*).

To evaluate the *in vivo* efficiency of therapeutic formulations, 4T1 and CT26 tumor cells were inoculated into the BALB/C mice and then tumor bulk and survival rate were measured following therapeutic interventions. The results

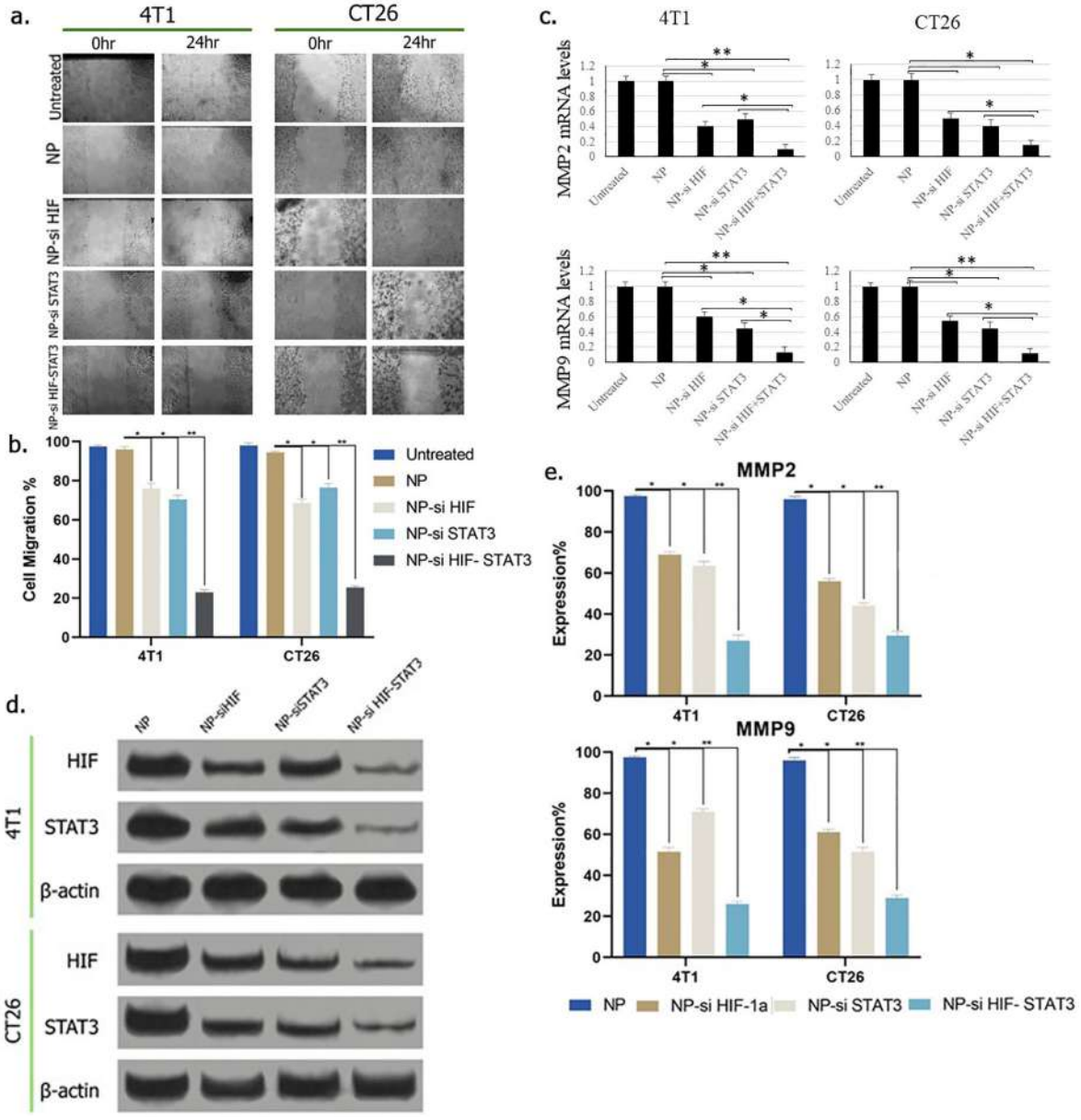

Figure 4. Simultaneous inhibition of HIF-1α and STAT3 suppressed the migratory potential and metastasis of CT26 and 4T1cancer cells. Evaluation of cancer cell migration after treatment with siRNA-loaded NPs was performed using the wound healing method **(A, B)**. The mRNA and protein expression levels of MMP2 and MMP9 were investigated by using the qPCR **(C)** and Western blot assays **(D** and **E)**.

revealed that in the treated groups with HIF-1α specific siRNA-NPs and STAT3 specific siRNA-NPs, tumor growth was considerably repressed. Moreover, concomitant inhibition of HIF-1α and STAT3 using siRNA-loaded SPION-TMC-ChT-TAT-H NPs synergistically resulted in greater inhibition of tumor development than in the single treated groups and control group (Figure 5, *B*).

Also, tumor survival was increased in mice treated with the therapeutic groups used in this study. As shown in Figure 5, *C*, dual delivery of siRNA molecules against HIF-1α and STAT3 using SPION-TMC-ChT-TAT-H nanocarriers remarkably prolonged the survival time in treated mice compared to single-treated and control mice.

In order to ensure the suppression of target molecules in tumor tissue, the expression of HIF-1α and STAT3 molecules in tumor samples was examined at the level of mRNA and protein. The results showed that siRNA loaded NPs could remarkably suppress the expression of both molecules in the tumor microenvironment (Figure 5, *D-F*).

Enumeration of CTLs demonstrated that inhibition of HIF-1α and STAT3 by NP-loaded siRNA alone partially increased the frequency of CTL and CD44-expressing CTLs in tumor, whereas dual-delivery of HIF-1α and STAT3 siRNA-loaded SPION-TMC-ChT-TAT-H NPs noticeably enhanced the CTL degranulation in tumor compared to the single-treated and control groups (Figure 5, *G* and *H*).

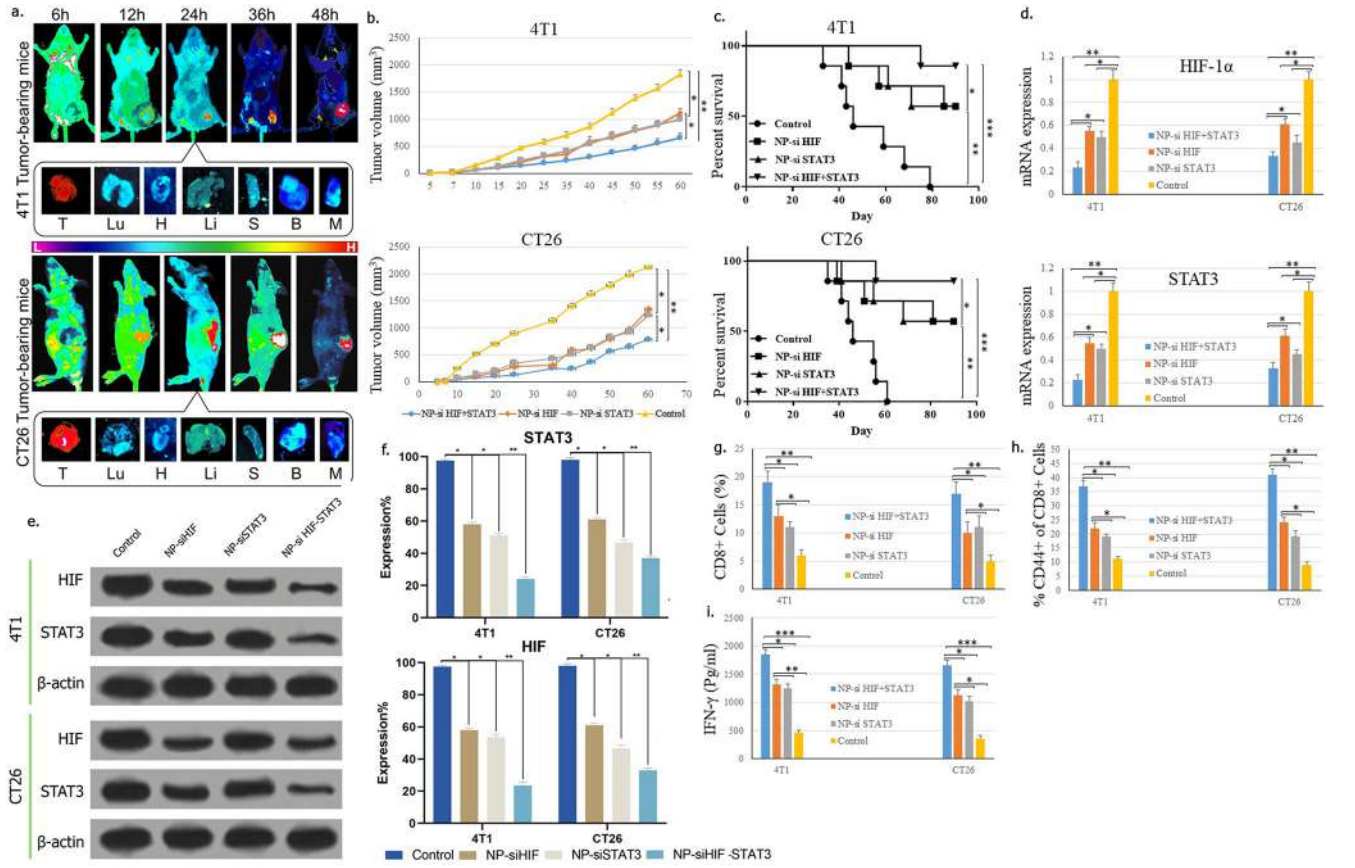

Figure 5. Treatment of tumor-bearing mice with SPION-TMC-ChT-TAT-H NPs loaded with HIF-1α/STAT3 specific siRNAs repressed the tumor expansion and increased the survival rate, and induced CTL response. Biodistribution of CY5-siRNA loaded NPs is shown in two different tumor models **(A)**. Tumor volume **(B)** and survival rate **(C)** of mice were evaluated in the tumor-bearing mice transfected with siRNA-loaded NPs. The expression of HIF-1α and STAT3 in tumor samples was analyzed by using qPCR and western blot assays **(D-F)**. The frequency of $CD8^+$ and CD44-expressing $CD8^+$ cells in tumor samples treated was examined using the flow cytometry **(G, H)**. The concentration of IFN-γ in supernatant of tumor-derived leukocytes after stimulation with tumor lysate was measured by ELISA **(F)**.

After that, the effect of the downregulation of target molecules on the IFNγ secretion was investigated in the supernatants of tumor-derived leukocytes stimulated by tumor antigen. The results demonstrated that single treatment with NP-HIF-1α-specific siRNA or NP-STAT3-specific siRNA moderately affected IFN-γ production. Nonetheless, combination treatment markedly increased the generation of this cytokine compared to control and mono treatment groups (Figure 5, *I*).

Discussion

The main purpose of this research was to establish a SPION-based siRNA delivery platform into cancer cells to suppress two important tumor-promoting factors in the tumor microenvironment, HIF-1α and STAT3, due to the remarkable characteristics of SPIONs that can be used in cancer treatment.[40] SPIONs have received much attention in gene delivery applications because of their low toxicity and a high ability for direct targeting using the exterior magnets. Accordingly, SPIONs can be applied as therapeutic and diagnostic agents due to their ideal properties.[41] In contrast, due to the agglomeration of SPION colloidal suspensions, their utilization in the clinic has been restricted.[42] Former studies have shown that coating SPION surface with some polymers such as dextran, chitosan, and polyethylene glycol can improve the disadvantages of SPION.[43] Therefore, in the current study, the SPION surface was coated with ChT and TMC to inhibit the agglomeration and raise solubility.[43] The use of these polymers could also enhance cellular uptake by increasing the compression of nucleic acids (DNA or RNA) into NPs.[44] Hyaluronate is a non-toxic biocompatible polymer that provides the conditions for chemical modification of NPs due to its high functional groups.[45] Besides, hyaluronic acid is also unique for developing gene/drug delivery systems against tumors expressing CD44.[46] Hyaluronate used in synthesized NPs can bind to CD44 receptors expressed in cancer cells and increase the cellular uptake of NPs.[47] Accordingly, Thomas et al evaluated the influence of hyaluronic acid on the cellular uptake capableness of SPIONs-PEG-HA and SPIONs-HA NPs and hyperthermia therapy in the $CD44^-$ NIH3T3 cells and $D44^+$ SCC7 cancer cells. They showed that the therapeutic effect of hyperthermia on NIH3T3 cells was negligible due to the lack of

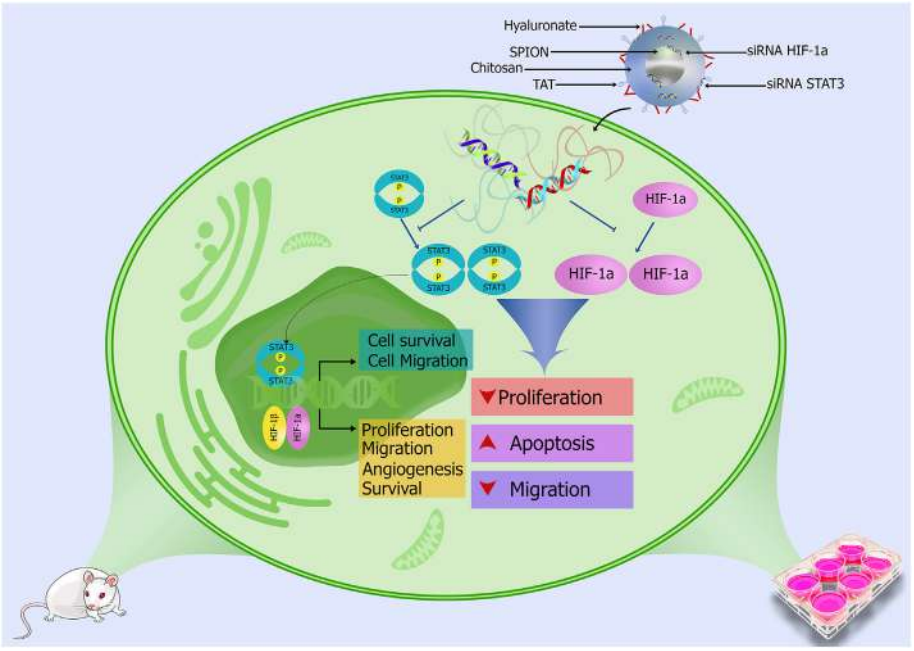

Figure 6. **(Graphical Abstract):** Concurrent inhibition of HIF-1α and STAT3 suppresses cancer development. Hyperactivity of HIF-1α and STAT3 leads to tumor growth by increasing the expression of factors involved in proliferation (Ki-67), metastasis (MMP2/9), *etc.* SPION-TMC-ChT-TAT-H NPs loaded with HIF-1α/STAT3 siRNAs effectively suppress tumor growth.

CD44 receptors and consequent poor uptake.[48] In another study, SPION loaded with micelle system was investigated for efficient transfer of foreign DNA to NIH3T3 and CT-26 cells using the poly (L-lysine) (PLL) as DNA vector and hyaluronic acid. The results of this study demonstrated that the use of PLL-HA-SPION micelles is effective in the treatment of hyperthermia based cancer and gene therapy guided by MR imaging in vivo.[45] Besides, Yang and colleagues conjugated hyaluronate to glycosaminoglycan-functionalized SPIONs using EDC activation and then used the resulting nanostructures to achieve better MRI quality and target HepG2 carcinoma cells.[49] Li et al stabilized the synthesized Fe3O4 NPs using polyethyleneimine (PEI) and then modified them with fluorescein isothiocyanate (FI) and HA with different molecular weights and prepared two different nanocomposites (Fe3O4-PEI-FI-HA6K and Fe3O4-PEI-FI-HA31K). They used then these NPs as functional probes for MR imaging of malignant cells *in vitro* and xenografted tumors *in vivo.*[50] A group of researchers used HA-SPION NPs for imaging and photothermal therapy (PTT) using near-infrared (NIR) laser irradiation in breast cancer. They indicated that HA-SPIONs were able to be rapidly infiltrated into HepG2 cells overexpressing CD44 receptors and accumulate considerably in tumor tissues.[51] Moreover, in this study, TAT peptide was used to develop the penetration of blood vessels and facilitate the efficiency of intracellular tumor uptake. As previously demonstrated, TAT acts as an enhancer in the delivery of various cargos through the cell membrane barriers and is derived from the HIV-1 Tat transduction domain.[52] Furthermore, conjugation of TAT peptide to the NPs can increase the surface charge of NPs to some extent due to the attendance of lysine and arginine residues in the peptide sequence.[53] TMC is a derivative of chitosan and a non-toxic, biocompatible polymer that exhibits high water solubility in a wide range of pH. TMC is also able to increase the loading amount of nucleic acids in NPs by having a high positive charge.[43] Moreover, the polymers used in this study protect the nucleic acids against degradation by extracellular enzymes and also help nucleic acid escape from the endolysosome.[54] Previous researches have demonstrated that SPION coverage with various polymers can enhance siRNA transfection efficacy. Accordingly, Luo et al efficiently silenced the PD-L1 gene in gastric cancer using siRNA/FA-PEG-SS-PEI-SPIONs system.[55] Another study showed that SPIONs modified by TMC, ChT, and CPPs are an effective platform for siRNA delivery and significantly inhibit the tumor growth *in vitro* and *in vivo.*[29] In other examination, SPIONs coated with TMC, radioisotope chelator of S-2-(4-isothiocyanatobenzyl)-1, 4, 7, 10-tetraazacyclododecane tetraacetic acid (DOTA), and targeting peptide of bombesin (BN) were designed and then labeled with ^{68}Ga. Finally prepared DOTA-BN-TMC-SPIONs nanostructure was tested as a PET/MRI probe for the detection of breast cancer both *in vitro*/*in vivo.*[56] Overall, we designed an efficient anti-HIF-1α/STAT3 siRNA delivery system based on SPION-TMC-ChT-TAT-H NPs in the 4T1 and CT26 carcinoma cell lines for the first time. In the next steps, we examined the concomitant inhibition effect of HIF-1α and STAT3 on cancer progression. We showed that blockade of HIF-1α/STAT3 axis inhibits tumor cell proliferation. Recent evidence has shown that continuous STAT3 activation increases the expression of Cycln D1, Survivin, and c-Myc, thereby accelerating cell cycle progression in colon and kidney cancers.[57,58] We also examined the inhibitory influence of STAT3 and HIF-1α on the apoptotic behaviors of neoplastic cells. Previous studies have reported that

activated STAT3 upregulates the expression of anti-apoptotic proteins such as Mcl, Bcl-2, and Bcl-XL to stop the apoptosis of multiple myeloma tumor cells. Thus, several studies proved that STAT3 inhibition leads to a reduction in cell proliferation in various cancers, including gastric, colon, breast, lung, and so on.[59–61] Chen et al reported that treatment of PC-3 prostate cancer cells using anti-HIF-1α miRNA significantly decreased the expression of anti-apoptotic Bcl-xL gene.[62] We also investigated the impact of HIF-1α and STAT3 silencing on the ability of cancer cells to migrate and metastasis. According to previous studies, continuous activation of STAT3 intensifies the expression of matrix metalloproteinases, such as MMP1 and MMP2/9.[63,64] Based on these findings, as well as preliminary evidence, STAT3 activation intensifies cell invasion, and inadequate STAT3 activity is also involved in migration, cell motility, and wound healing.[65,66] Many studies have shown that the hypoxic environment and the HIF-1α molecule increase the levels of MMPs and metastasis in breast and lung cancer.[67,68] In this study, the results of the scratch method and the reduction of MMP2/MMP9 expression levels verified that the co-inhibition of HIF-1α/STAT3 suppressed the migratory performance of CT26 and 4T1 cancer cells. Also, in one of our recent studies, the HIF-1α / EP4 axis was inhibited in breast, colon, and melanoma murine cancer cells using SPIONs-TMC-HA nanocarriers encapsulated with specific siRNA against HIF-1α and E7046 (EP4 antagonist). Besides, this designed nanocomposite with ideal physicochemical properties remarkably impeded the expression of the MMPs gene and thus reduced the rate of migration in this malignant cells.[69] We also performed *in vivo* assays to evaluate the antitumor activity of the produced nanocarriers. As displayed in Figure 5, tumor volume was remarkably reduced in tumor-bearing mice treated with NPs-loaded with HIF-1α/STAT3 siRNA. Moreover, after treating the mice with this therapeutic formulation, the survival rate was greatly improved. Since the response of CTLs is the most important pillar of the immune system's response to cancer cells, the frequency of these cells and their activity were also evaluated in treated mice. The results showed that concomitant inhibition of HIF-1α/STAT3 significantly enhanced CTL frequency and function indicating the remarkable induction of tumor-eradicating immune responses. Generally, these findings indicated that SPION-TMC-ChT-TAT-H NPs loaded with siRNAs against HIF-1α/STAT3 could be suggested as a potential cancer therapeutic protocol in repressing HIF-1α and STAT3 expression (Figure 6).

Acknowledgment

We would like to thank Mr. Payam Ashrafi and Mrs. Negar Alizadeh for their excellent technical contribution.

Appendix A. Supplementary data

Supplementary data to this article can be found online at https://doi.org/10.1016/j.nano.2021.102373.

References

1. Baghban R, Roshangar L, Jahanban-Esfahlan R, Seidi K, Ebrahimi-Kalan A, Jaymand M, et al. Tumor microenvironment complexity and therapeutic implications at a glance. *Cell Communication Signaling* 2020;**18**:1-19.
2. Whiteside TJ. The tumor microenvironment and its role in promoting tumor growth. *Oncogene* 2008;**27**:5904-12.
3. Kessenbrock K, Plaks V, Werb ZJ. Matrix metalloproteinases: regulators of the tumor microenvironment. *Cell* 2010;**141**:52-67.
4. Esmaily M, Masjedi A, Hallaj S, Nabi Afjadi M, Malakotikhah F, Ghani S, et al. Blockade of CTLA-4 increases anti-tumor response inducing potential of dendritic cell vaccine. *J Control Release* 2020;**326**:63-74.
5. Hassannia H, Ghasemi Chaleshtari M, Atyabi F, Nosouhian M, Masjedi A, Hojjat-Farsangi M, et al. Blockage of immune checkpoint molecules increases T-cell priming potential of dendritic cell vaccine. *Immunology* 2020;**159**:75-87.
6. Masjedi A, Ahmadi A, Atyabi F, Farhadi S, Irandoust M, Khazaei-Poul Y, et al. Silencing of IL-6 and STAT3 by siRNA loaded hyaluronate-N,N,N-trimethyl chitosan nanoparticles potently reduces cancer cell progression. *Int J Biol Macromol* 2020;**149**:487-500.
7. Masjedi A, Ahmadi A, Ghani S, Malakotikhah F, Nabi Afjadi M, Irandoust M, et al. Silencing adenosine A2a receptor enhances dendritic cell-based cancer immunotherapy. *Nanomedicine* 2020;**29**:102240.
8. Jadidi-Niaragh F, Atyabi F, Rastegari A, Kheshtchin N, Arab S, Hassannia H, et al. CD73 specific siRNA loaded chitosan lactate nanoparticles potentiate the antitumor effect of a dendritic cell vaccine in 4T1 breast cancer bearing mice. *J Control Release* 2017;**246**:46-59.
9. Hajizadeh F, Okoye I, Esmaily M, Ghasemi Chaleshtari M, Masjedi A, Azizi G, et al. Hypoxia inducible factors in the tumor microenvironment as therapeutic targets of cancer stem cells. *Life Sci* 2019;**237**:116952.
10. Hu C-J, Wang L-Y, Chodosh LA, Keith B, Simon MCJ. Differential roles of hypoxia-inducible factor 1α (HIF-1α) and HIF-2α in hypoxic gene regulation. *Molecular cellular biology* 2003;**23**:9361-74.
11. Keith B, Johnson RS, Simon MCJ. HIF1α and HIF2α: sibling rivalry in hypoxic tumour growth and progression. *Nat Rev Cancer* 2012;**12**:9-22.
12. Semenza GLJ. Hypoxia-inducible factors in physiology and medicine. *Cell* 2012;**148**:399-408.
13. Bromberg J, Darnell JEJ. The role of STATs in transcriptional control and their impact on cellular function. *Oncogene* 2000;**19**:2468-73.
14. Lee MY, Joung YH, Lim EJ, Park J-H, Ye S-K, Park T, et al. Phosphorylation and activation of STAT proteins by hypoxia in breast cancer cells. *The Breast* 2006;**15**:187-95.
15. Aggarwal BB, Sethi G, Ahn KS, Sandur SK, Pandey MK, Kunnumakkara AB, et al. Targeting signal-transducer-and-activator-of-transcription-3 for prevention and therapy of cancer: modern target but ancient solution. *Ann N Y Acad Sci* 2006;**1091**:151-69.
16. Kang S-H, Yu MO, Park K-J, Chi S-G, Park D-H, Chung Y-GJ. Activated STAT3 regulates hypoxia-induced angiogenesis and cell migration in human glioblastoma. *Neurosurgery* 2010;**67**:1386-95.
17. Jung JE, Lee HG, Cho IH, Chung DH, Yoon SH, Yang YM, et al. STAT3 is a potential modulator of HIF-1-mediated VEGF expression in human renal carcinoma cells. *FASEB J* 2005;**19**:1296-8.
18. Jung JE, Kim HS, Lee CS, Shin Y-J, Kim Y-N, Kang G-H, et al. STAT3 inhibits the degradation of HIF-1α by pVHL-mediated ubiquitination. *Experimental molecular medicine* 2008;**40**:479-85.
19. Finger EC, Giaccia AJJ. Hypoxia, inflammation, and the tumor microenvironment in metastatic disease. *Cancer Metastasis Rev* 2010;**29**:285-93.
20. Eid M, El-Hallouty S, El-Manawaty M, Abdelzaher FJ. Physicochemical characterization and biocompatibility of SPION@ Plasmonic@ chitosan core-shell nanocomposite biosynthesized from fungus species. *Journal of Nanomaterials* 2019;**2019**.
21. Silva AC, Oliveira TR, Mamani JB, Malheiros SM, Malavolta L, Pavon LF, et al. Application of hyperthermia induced by superparamagnetic

iron oxide nanoparticles in glioma treatment. *Int J Nanomedicine* 2011;**6**:591.
22. Muthiah M, Park I-K, Cho C-SJ. Surface modification of iron oxide nanoparticles by biocompatible polymers for tissue imaging and targeting. *Biotechnol Adv* 2013;**31**:1224-36.
23. Almalik A, Benabdelkamel H, Masood A, Alanazi IO, Alradwan I, Majrashi MA, et al. Hyaluronic acid coated chitosan nanoparticles reduced the immunogenicity of the formed protein corona. *Sci Rep* 2017;**7**:10542.
24. Jones SW, Christison R, Bundell K, Voyce CJ, Brockbank SM, Newham P, et al. Characterisation of cell-penetrating peptide-mediated peptide delivery. *Br J Pharmacol* 2005;**145**:1093.
25. F. Hosseini, A. Mahdian-Shakib, F. Jadidi-Niaragh, S. E. Enderami, H. Mohammadi, M. Hemmatzadeh, et al., Anti-inflammatory and anti-tumor effects of alpha-l-guluronic acid (G2013) on cancer-related inflammation in a murine breast cancer model. *Biomedicine & pharmacotherapy = Biomedecine & pharmacotherapie*. 2018;**98**:793–800
26. Hosseini F, Hassannia H, Mahdian-Shakib A, Jadidi-Niaragh F, Enderami SE, Fattahi M, et al. Targeting of crosstalk between tumor and tumor microenvironment by β-D mannuronic acid (M2000) in murine breast cancer model. *Cancer Med* 2017;**6**:640-50.
27. Mu B, Liu P, Dong Y, Lu C, Wu XJ. Superparamagnetic pH-sensitive multilayer hybrid hollow microspheres for targeted controlled release. *J Polym Sci A Polym Chem* 2010;**48**:3135-44.
28. Atyabi F, Majzoob S, Iman M, Salehi M, Dorkoosh FJ. In vitro evaluation and modification of pectinate gel beads containing trimethyl chitosan, as a multi-particulate system for delivery of water-soluble macromolecules to colon. *Carbohydr Polym* 2005;**61**:39-51.
29. Hajizadeh F, Ardebili SM, Moornani MB, Masjedi A, Atyabi F, Kiani M, et al. Silencing of HIF-1α/CD73 axis by siRNA-loaded TAT-chitosan-spion nanoparticles robustly blocks cancer cell progression. *Eur J Pharmacol* 2020;**173235**.
30. Ghasemi-Chaleshtari M, Kiaie SH, Irandoust M, Karami H, Nabi Afjadi M, Ghani S, et al. Concomitant blockade of A2AR and CTLA-4 by siRNA-loaded polyethylene glycol-chitosan-alginate nanoparticles synergistically enhances antitumor T-cell responses. *J Cell Physiol* 2020.
31. Nikkhoo A, Rostami N, Farhadi S, Esmaily M, Moghadaszadeh Ardebili S, Atyabi F, et al. Codelivery of STAT3 siRNA and BV6 by carboxymethyl dextran trimethyl chitosan nanoparticles suppresses cancer cell progression. *Int J Pharm* 2020;**581**:119236.
32. Hashemi V, Ahmadi A, Malakotikhah F, Chaleshtari MG, Baghi Moornani M, Masjedi A, et al. Silencing of p68 and STAT3 synergistically diminishes cancer progression. *Life Sci* 2020;**249**:117499.
33. Izadi S, Moslehi A, Kheiry H, Kiani FK, Ahmadi A, Masjedi A, et al. Codelivery of HIF-1α siRNA and dinaciclib by carboxylated graphene oxide-trimethyl chitosan-hyaluronate nanoparticles significantly suppresses cancer cell progression. *Pharm Res* 2020;**37**:1-20.
34. Ghalamfarsa G, Rastegari A, Atyabi F, Hassannia H, Hojjat-Farsangi M, Ghanbari A, et al. Anti-angiogenic effects of CD73-specific siRNA-loaded nanoparticles in breast cancer-bearing mice. *J Cell Physiol* 2018;**233**:7165-77.
35. Hashemi V, Ahmadi A, Malakotikhah F, Chaleshtari MG, Moornani MB, Masjedi A, et al. Silencing of p68 and STAT3 synergistically diminishes cancer progression. *Life Sci* 2020;**117499**.
36. F. Jadidi-Niaragh, M. Jeddi-Tehrani, B. Ansaripour, S. M. Razavi, R. A. Sharifian and F. Shokri, Reduced frequency of NKT-like cells in patients with progressive chronic lymphocytic leukemia. *Medical oncology (Northwood, London, England)*. 2012;**29**:3561–9
37. Kheshtchin N, Arab S, Ajami M, Mirzaei R, Ashourpour M, Mousavi N, et al. Inhibition of HIF-1α enhances anti-tumor effects of dendritic cell-based vaccination in a mouse model of breast cancer. *Cancer Immunol Immunother* 2016;**65**:1159-67.
38. Gunetti M, Castiglia S, Rustichelli D, Mareschi K, Sanavio F, Muraro M, et al. Validation of analytical methods in GMP: the disposable Fast Read 102® device, an alternative practical approach for cell counting. *J Transl Med* 2012;**10**:112.
39. Yao Y, Luo F, Tang C, Chen D, Qin Z, Hua W, et al. Molecular subgroups and B7-H4 expression levels predict responses to dendritic cell vaccines in glioblastoma: an exploratory randomized phase II clinical trial. *Cancer Immunol Immunother* 2018;**67**:1777-88.
40. Hosseini M, Haji-Fatahaliha M, Jadidi-Niaragh F, Majidi J, Yousefi M. The use of nanoparticles as a promising therapeutic approach in cancer immunotherapy. *Artif Cells Nanomed Biotechnol* 2016;**44**:1051-61.
41. Al-Deen FN, Selomulya C, Ma C, Coppel RL. Superparamagnetic nanoparticle delivery of DNA vaccine *DNA Vaccines. Springer, pp* 2014:181-94.
42. Sharifi S, Seyednejad H, Laurent S, Atyabi F, Saei AA, Mahmoudi MJ. Superparamagnetic iron oxide nanoparticles for in vivo molecular and cellular imaging. *Contrast media molecular imaging* 2015;**10**:329-55.
43. Kamalzare S, Noormohammadi Z, Rahimi P, Atyabi F, Irani S, Tekie FSM, et al. Carboxymethyl dextran-trimethyl chitosan coated superparamagnetic iron oxide nanoparticles: an effective siRNA delivery system for HIV-1 Nef. *J Cell Physiol* 2019;**234**:20554-65.
44. M. Stovall, S. A. Smith, B. M. Langholz, J. D. Boice Jr, R. E. Shore, M. Andersson, et al., Dose to the contralateral breast from radiotherapy and risk of second primary breast cancer in the WECARE study. *International Journal of Radiation Oncology* Biology* Physics*. 2008;**72**:1021–1030
45. Thomas RG, Muthiah M, Moon M, Park I-K, Jeong YYJ. SPION loaded poly (L-lysine)/hyaluronic acid micelles as MR contrast agent and gene delivery vehicle for cancer theranostics. *Macromolecular Research* 2017;**25**:446-51.
46. Saravanakumar G, Deepagan V, Jayakumar R, Park JHJ. Hyaluronic acid-based conjugates for tumor-targeted drug delivery and imaging. *J Biomed Nanotechnol* 2014;**10**:17-31.
47. Jung HS, Kong WH, Sung DK, Lee M-Y, Beack SE, Keum DH, et al. Nanographene oxide–hyaluronic acid conjugate for photothermal ablation therapy of skin cancer. *ACS Nano* 2014;**8**:260-8.
48. Thomas RG, Moon MJ, Lee H, Sasikala ARK, Kim CS, Park I-K, et al. Hyaluronic acid conjugated superparamagnetic iron oxide nanoparticle for cancer diagnosis and hyperthermia therapy. *Carbohydr Polym* 2015;**131**:439-46.
49. Yang R-M, Fu C-P, Li N-N, Wang L, Xu X-D, Yang D-Y, et al. Glycosaminoglycan-targeted iron oxide nanoparticles for magnetic resonance imaging of liver carcinoma. *Mater Sci Eng C* 2014;**45**:556-63.
50. Li J, He Y, Sun W, Luo Y, Cai H, Pan Y, et al. Hyaluronic acid-modified hydrothermally synthesized iron oxide nanoparticles for targeted tumor MR imaging. *Biomaterials* 2014;**35**:3666-77.
51. Yang R-M, Fu C-P, Fang J-Z, Xu X-D, Wei X-H, Tang W-J, et al. Hyaluronan-modified superparamagnetic iron oxide nanoparticles for bimodal breast cancer imaging and photothermal therapy. *Int J Nanomedicine* 2017;**12**:197.
52. Liu E, Zhang M, Cui H, Gong J, Huang Y, Wang J, et al. Tat-functionalized ag-Fe3O4 nano-composites as tissue-penetrating vehicles for tumor magnetic targeting and drug delivery. *Acta pharmaceutica sinica B* 2018;**8**:956-68.
53. Rahmat D, Khan MI, Shahnaz G, Sakloetsakun D, Perera G, Bernkop-Schnürch AJ. Synergistic effects of conjugating cell penetrating peptides and thiomers on non-viral transfection efficiency. *Biomaterials* 2012;**33**:2321-6.
54. Nimesh S, Gupta N, Chandra RJ. Cationic polymer based nanocarriers for delivery of therapeutic nucleic acids. *J Biomed Nanotechnol* 2011;**7**:504-20.
55. Luo X, Peng X, Hou J, Wu S, Shen J, Wang LJ. Folic acid-functionalized polyethylenimine superparamagnetic iron oxide nanoparticles as theranostic agents for magnetic resonance imaging and PD-L1 siRNA delivery for gastric cancer. *Int J Nanomedicine* 2017;**12**:5331.
56. Hajiramezanali M, Atyabi F, Mosayebnia M, Akhlaghi M, Geramifar P, Jalilian AR, et al. 68Ga-radiolabeled bombesin-conjugated to trimethyl chitosan-coated superparamagnetic nanoparticles for molecular imaging:

preparation, characterization and biological evaluation. *Int J Nanomedicine* 2019;**14**:2591.
57. Lin L, Liu A, Peng Z, Lin H-J, Li P-K, Li C, et al. STAT3 is necessary for proliferation and survival in colon cancer-initiating cells. *Cancer Res* 2011;**71**:7226-37.
58. Corvinus FM, Orth C, Moriggl R, Tsareva SA, Wagner S, Pfitzner EB, et al. Persistent STAT3 activation in colon cancer is associated with enhanced cell proliferation and tumor growth. *Neoplasia* 2005;**7**:545.
59. Kanai M, Konda Y, Nakajima T, Izumi Y, Kanda N, Nanakin A, et al. Differentiation-inducing factor-1 (DIF-1) inhibits STAT3 activity involved in gastric cancer cell proliferation via MEK-ERK-dependent pathway. *Oncogene* 2003;**22**:548-54.
60. Pancotti F, Roncuzzi L, Maggiolini M, Gasperi-Campani AJ. Caveolin-1 silencing arrests the proliferation of metastatic lung cancer cells through the inhibition of STAT3 signaling. *Cell Signal* 2012;**24**:1390-7.
61. Chen H, Yang Z, Ding C, Chu L, Zhang Y, Terry K, et al. Discovery of O-alkylamino-tethered niclosamide derivatives as potent and orally bioavailable anticancer agents. *ACS Med Chem Lett* 2013;**4**:180-5.
62. Chen N, Chen X, Huang R, Zeng H, Gong J, Meng W, et al. BCL-xL is a target gene regulated by hypoxia-inducible factor-1α. *J Biol Chem* 2009;**284**:10004-12.
63. Dechow TN, Pedranzini L, Leitch A, Leslie K, Gerald WL, Linkov I, et al. Requirement of matrix metalloproteinase-9 for the transformation of human mammary epithelial cells by Stat3-C. *Proc Natl Acad Sci* 2004;**101**:10602-7.
64. Itoh M, Murata T, Suzuki T, Shindoh M, Nakajima K, Imai K, et al. Requirement of STAT3 activation for maximal collagenase-1 (MMP-1) induction by epidermal growth factor and malignant characteristics in T24 bladder cancer cells. *Oncogene* 2006;**25**:1195.
65. Silver DL, Naora H, Liu J, Cheng W, Montell DJJ. Activated signal transducer and activator of transcription (STAT) 3: localization in focal adhesions and function in ovarian cancer cell motility. *Cancer Res* 2004;**64**:3550-8.
66. Sano S, Itami S, Takeda K, Tarutani M, Yamaguchi Y, Miura H, et al. Keratinocyte-specific ablation of Stat3 exhibits impaired skin remodeling, but does not affect skin morphogenesis. *EMBO J* 1999;**18**:4657-68.
67. Choi JY, Jang YS, Min SY, Song JYJ. Overexpression of MMP-9 and HIF-1α in breast cancer cells under hypoxic conditions. *J Breast Cancer* 2011;**14**:88-95.
68. Liang H, Gu M, Yang C, Wang H, Wen X, Zhou QJ. Sevoflurane inhibits invasion and migration of lung cancer cells by inactivating the p38 MAPK signaling pathway. *J Anesth* 2012;**26**:381-92.
69. Karpisheh V, Afjedi JF, Afjadi MN, Haeri MS, Sough TSA, Asl SH, et al. Inhibition of HIF-1α/EP4 axis by hyaluronate-trimethyl chitosan-SPION nanoparticles markedly suppresses the growth and development of cancer cells. *Int J Biol Macromol* 2020.